The Canadian Mineralogist
Vol. 40, pp. 1657-1673 (2002)

SCANDIUM MINERALOGY: PRETULITE WITH SCANDIAN ZIRCON AND XENOTIME-(Y) WITHIN AN APATITE-RICH OOLITIC IRONSTONE FROM SAINT-AUBIN-DES-CHÂTEAUX, ARMORICAN MASSIF, FRANCE

YVES MOËLO§

Laboratoire de Chimie des Solides, Institut des Matériaux Jean Rouxel (*UMR CNRS 6502*),
2, rue de la Houssinière, BP 32229, F-44322 Nantes Cedex 3, France

YVES LULZAC

Laboratoire de Gemmologie, Université de Nantes, 2, rue de la Houssinière, BP 9208, F-44322 Nantes Cedex 3, France

OLIVIER ROUER

Institut des Sciences de la Terre d'Orléans (*UMR CNRS-Université C 6113*),
1A, rue de la Férollerie, F-45071 Orléans Cedex 2, France

PIERRE PALVADEAU

Laboratoire de Chimie des Solides, Institut des Matériaux Jean Rouxel (*UMR CNRS 6502*),
2, rue de la Houssinière, BP 32229, F-44322 Nantes Cedex 3, France

ÉRIC GLOAGUEN*

Laboratoire de Minéralogie, Muséum National d'Histoire Naturelle, Unité CNRS FREE 2456,
61 rue Buffon, F-75005 Paris, France

PHILIPPE LÉONE

Laboratoire de Chimie des Solides, Institut des Matériaux Jean Rouxel (*UMR CNRS 6502*),
2, rue de la Houssinière, BP 32229, F-44322 Nantes Cedex 3, France

ABSTRACT

The scandium phosphate pretulite has been identified with scandian zircon and xenotime-(Y) in an apatite-rich oolitic Ordovician ironstone at Saint-Aubin-des-Châteaux, Armorican Massif, France. Pseudo-octahedral crystals of pretulite, up to 400 μm across, have grown epitactically on detrital zircon. They reveal complex zoning due to incorporation of Y and *HREE*, as well as to an extended solid-solution toward the zircon end-member. Characteristic compositions in the pretulite – xenotime-(Y) – zircon system are: $Prl_{0.973}Xnt_{0.020}Zrn_{0.007}$, $Prl_{0.907}Xnt_{0.088}Zrn_{0.005}$, $Prl_{0.873}Xnt_{0.042}Zrn_{0.085}$, $Prl_{0.718}Xnt_{0.024}Zrn_{0.258}$ and $Prl_{0.453}Xnt_{0.042}Zrn_{0.505}$. A single-crystal X-ray refinement of the structure in space group $I4_1/amd$ ($R = 0.0389$) gives a 6.5870(9), c 5.809(1) Å, for the formula $(Sc_{0.904}Y_{0.032}HREE_{0.016}Zr_{0.048})(P_{0.952}Si_{0.048})O_4$. The Raman spectrum is presented. Detrital zircon shows phosphate-rich metamict zones containing *HREE* and Sc (up to 3.2 wt.% Sc_2O_3). Analytical and crystallographic data suggest a complete solid-solution between zircon and pretulite. Xenotime-(Y), also epitactic on zircon, shows distinct stages of crystallization, with a decrease in Y together with an enrichment in the lighter *REE* and Sc (up to 0.7 wt.% Sc_2O_3). The scandium minerals at Saint-Aubin reflect the evolution of the iron ore, from sedimentation to diagenesis and metamorphism, followed by multistage hydrothermal leaching and recrystallization. Despite the high concentration of Fe in the environment, this quite unique occurrence of Sc minerals illustrates the high capacity of the phosphate ion to extract scandium and precipitate it as a specific phase, at relatively low-temperature conditions.

Keywords: scandium, phosphate, pretulite, zircon, xenotime-(Y), iron ore, Ordovician, Armorican Massif, France.

§ *E-mail address*: moelo@cnrs-imn.fr
* *Present address*: Institut des Sciences de la Terre d'Orléans (UMR CNRS-Université C 6113), 1A, rue de la Férollerie, F-45071 Orléans Cedex 2, France

Sommaire

Un phosphate de scandium, la prétulite, a été identifié, en association avec du zircon et du xénotime-(Y) scandifères, dans un minerai de fer oolithique ordovicien riche en apatite à Saint-Aubin-des-Châteaux, Massif Armoricain, en France. Les cristaux pseudo-octaédriques de prétulite (jusqu'à 400 μm) sont en surcroissance épitaxique sur du zircon détritique. Ils montrent une zonation complexe due à l'incorporation du Y et des terres rares lourdes, ainsi qu'à une solution solide étendue vers le pôle zircon. Des compositions-types dans le système prétulite – xénotime-(Y) – zircon sont: $Prl_{0.973}Xnt_{0.020}Zrn_{0.007}$, $Prl_{0.907}Xnt_{0.088}Zrn_{0.005}$, $Prl_{0.873}Xnt_{0.042}Zrn_{0.085}$, $Prl_{0.718}Xnt_{0.024}Zrn_{0.258}$ et $Prl_{0.453}Xnt_{0.042}Zrn_{0.505}$. L'affinement de la structure cristalline aux rayons X sur monocristal (groupe spatial $I4_1/amd$, R = 0,0389) a été faite avec a 6,5870(9), c 5,809(1) Å, sur la base de la formule $(Sc_{0.904}Y_{0.032}TRL_{0.016}Zr_{0.048})(P_{0.952}Si_{0.048})O_4$. Le spectre Raman est présenté. Le zircon détritique montre des zones métamictes riches en phosphate, avec terres rares lourdes (*TRL*) et scandium (jusqu'à 3,2% pds Sc_2O_3). Les données tant analytiques que cristallographiques suggèrent une solution solide complète entre prétulite et zircon. Le xénotime-(Y), également en épitaxie sur le zircon, montre plusieurs stades de cristallisation, traduisant un appauvrissement en Y corrélatif d'un enrichissement en faveur de terres rares plus légères, ainsi qu'en scandium (jusqu'à 0,7% pds Sc_2O_3). La minéralogie du scandium à Saint-Aubin reflète l'évolution du minerai de fer: sédimentation, diagenèse et métamorphisme, et enfin lessivage et recristallisation par des venues hydrothermales polyphasées. Malgré la haute concentration en fer de l'environnement, cette occurrence très particulière illustre la forte capacité de l'ion phosphate à se combiner au scandium et à le précipiter sous forme d'une phase minérale spécifique à relativement basse température.

Mots-clés: scandium, phosphate, prétulite, zircon, xénotime-(Y), minerai de fer, Ordovicien, Massif Armoricain, France.

Introduction

Scandium is rarely expressed as specific mineral species, owing to its dilution in common silicates, where it substitutes for Fe, Mg and Al. There exist at present only nine approved species of scandium minerals: six silicates (bazzite, thortveitite, cascandite, jervisite, scandiobabingtonite and kristiansenite), and three phosphates (kolbeckite, pretulite and juonniite) (Mellini *et al.* 1982, Orlandi *et al.* 1998, Hey *et al.* 1982, Bernhard *et al.* 1998b, Liferovich *et al.* 1997, Raade *et al.* 2002).

Pretulite was discovered at Höllkogel, in eastern Austria, by Bernhard *et al.* (1998b), who described numerous occurrences within quartz–lazulite veins in the Lower Austro-alpine Grobneis complex. Another probable occurrence of pretulite was incompletely described as an unnamed Sc phosphate by Novák & Srein (1989) in the Dolní Bory pegmatites of western Moravia, Czech Republic. The present study deals with a new occurrence of pretulite, identified in a sandstone quarry located at Saint-Aubin-des-Châteaux, Loire-Atlantique, in western France. Here, pretulite is closely associated with scandian zircon and xenotime-(Y) within a sedimentary iron ore showing a complex paragenetic evolution. This occurrence presents new insight concerning aspects of the geochemistry and crystal chemistry of scandium.

Geological Setting and Petrology

Figure 1 gives the geographic location of the quarry of Saint-Aubin-des-Châteaux. This quarry is situated in the lower member of the Grès armoricain Formation, of Arenigian age. This member is mainly composed of sandstone; at a regional scale, it includes oolitic ironstones (Chauvel 1974) at four main horizons, A to D, from top to bottom. These ironstones have been mined in the past (Puzenat 1939). According to Chauvel (1974), they are essentially composed of iron oxides (magnetite, hematite, ilmenite), silicates (chlorite, stilpnomelane) and quartz, siderite, pyrite and apatite. The phosphate is ubiquitous (mean concentration over 2 wt.%; up to 6 wt.% in the B horizon).

In the Saint-Aubin quarry, only the A horizon is well developed. It is mainly composed of siderite and chlorite, but locally very enriched in Sr-bearing fluorapatite (4 wt.% SrO: Chauvel & Phan 1965). It was affected by diagenesis and very low grade metamorphism. The primary sedimentary features, where preserved, consist of millimetric layers of oolites. Some of these layers are enriched in fluorapatite (abundant), or minor detrital

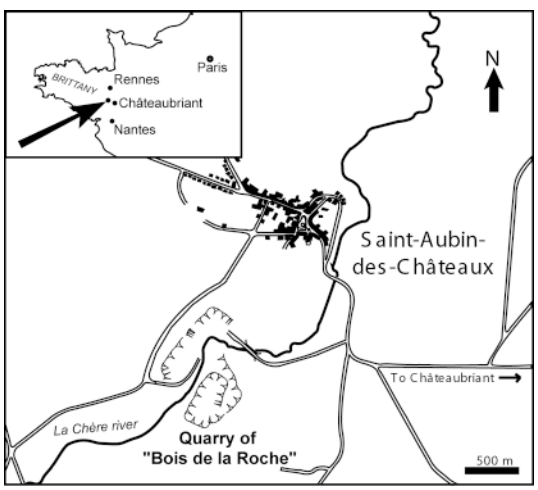

FIG. 1. Geographic location of the Bois-de-la-Roche quarry at Saint-Aubin-des-Châteaux (arrow on the inset map).

titanium oxides and zircon. Carbonaceous phases (organic matter and late graphite) are disseminated throughout the rock, giving it a characteristic black color. SEM examinations reveal rare minute crystals of galena, sphalerite and monazite-(Ce). Pretulite and xenotime-(Y) are only present as epitactic overgrowths on zircon crystals.

The primary texture was later altered by hydrothermal processes (at least three stages of hydrothermal activity), as indicated notably by the presence of massive pyrite, together with minor base-metal sulfides like marcasite, galena, and sphalerite (Herrouin *et al.* 1989, Moëlo *et al.* 2000, Gloaguen 2002). Centimetric to decimetric veinlets of quartz, siderite, pyrite and lulzacite (a recently described Sr–Al–Fe phosphate: Moëlo *et al.* 2000, Léone *et al.* 2000) were formed within the ironstone (incorrectly called "limestone" in Moëlo *et al.* 2000). Hydrothermal processes have also transformed the ironstone itself locally by recrystallization of siderite, dissolution and recrystallization of Sr-rich fluorapatite, crystallization of graphite lamellae at the expense of organic matter, and formation of a red-brown variety of chlorite.

Pretulite

Descriptive aspects

Pretulite was first discovered in an apatite-rich fragment from the A horizon, showing numerous submillimetric hexagonal platelets of "red-brown chlorite" (a Mg-poor, Al-rich chamosite). This fragment was dissolved in HCl; the whole residue contains a dozen crystals of pretulite with a flattened pseudo-octahedral habit (Fig. 2). The main form is the bipyramid {011}, with subordinate basal faces {001}; faces of the prismatic form {110} are rare. The size of these crystals varies from 150 to 400 μm across; they are translucent, yellowish white, with an adamantine luster.

In polished section, one of these crystal appears to be an overgrowth on a rounded crystal of zircon (Fig. 3); xenotime-(Y) also is present. Thin sections made of samples of the A horizon show other crystals of pretulite, invariably as an epitactic overgrowth on zircon crystals (Fig. 4); gangue minerals are chamosite with fluorapatite and graphite.

Chemical characterization

Imaging by scanning electron microscopy (SEM) and with back-scattered electrons (BSE) invariably reveals the presence of chemical zoning in the crystals of pretulite. Figure 3 reveals a complex pattern of growth-induced zoning, showing schematically first a dark grey core (A zone), secondly, a narrow intermediate rim (B zone, light grey), then a wide grey outer zone (C zone), and finally (at the opposite side) a thinner white layer located close to the zircon crystal (D zone). These zones were characterized chemically by elemental mapping and quantitative electron-probe micro-analysis (EPMA; Figs. 5a-d, Table 1).

In the A zone (anal. 1–7), the pretulite is the richest in Sc, with low contents of yttrium (1.2 to 3.0 wt.% Y_2O_3) and heavy rare-earth elements (*HREE*) (mostly

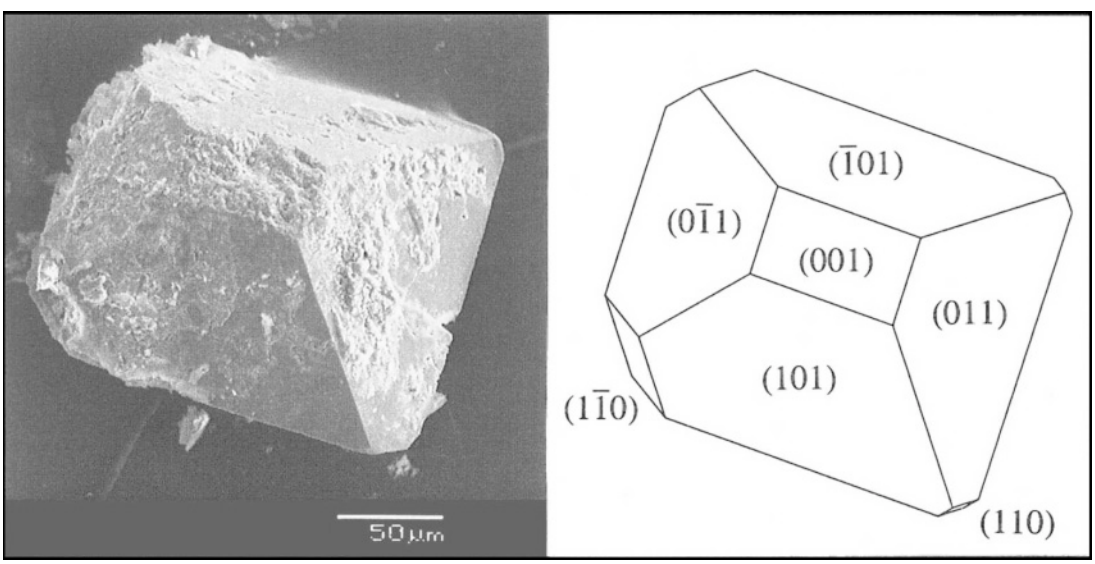

FIG. 2. SEM–BSE image of a euhedral crystal of pretulite (left), and proposed crystal forms (right): combination of main {011} bipyramid with minor {001} and rare {110}.

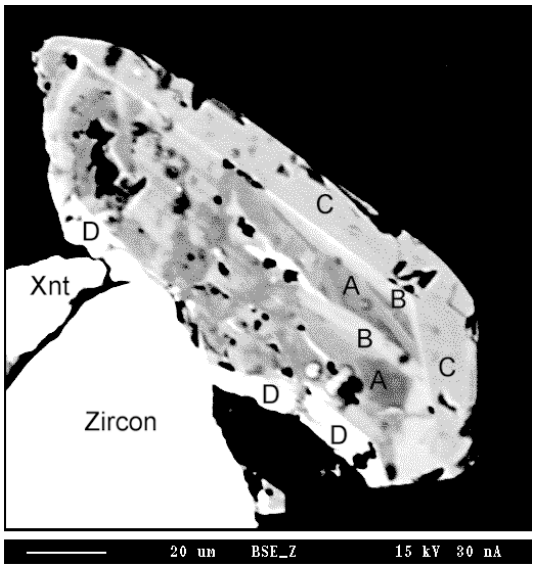

FIG. 3. Overgrowth of a zoned crystal of pretulite (~150 × 50 μm), together with a crystal of xenotime-(Y) (*Xnt*) over a detrital zircon crystal. SEM-BSE image of a polished section. Central zone A (dark grey): REE- and (Zr, Si)-poor pretulite; intermediate zone B (light grey) enriched in REE and (Zr, Si); zone C (medium grey, upper and right border): REE-rich pretulite; zone D (white rim close to zircon): (Zr, Si)-rich pretulite.

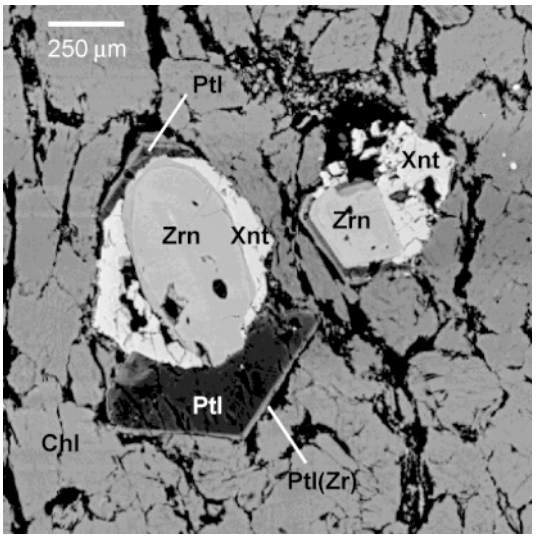

FIG. 4. Epitactic overgrowth of euhedral pretulite (Ptl, grey-black), with an external Zr-rich rim [Ptl(Zr), light grey) at the two opposite ends of a detrital crystal of zircon (Zrn, light grey). The white zones correspond to an epitactic overgrowth of xenotime-(Y) (Xnt). Chlorite (Chl) with graphite lamellae (within black area) is the matrix mineral. A smaller zircon – xenotime-(Y) – pretulite aggregate is visible at right. SEM–BSE image; for clarity, the contrast between the central part [zircon and xenotime-(Y)] and the rest of the image has been attenuated.

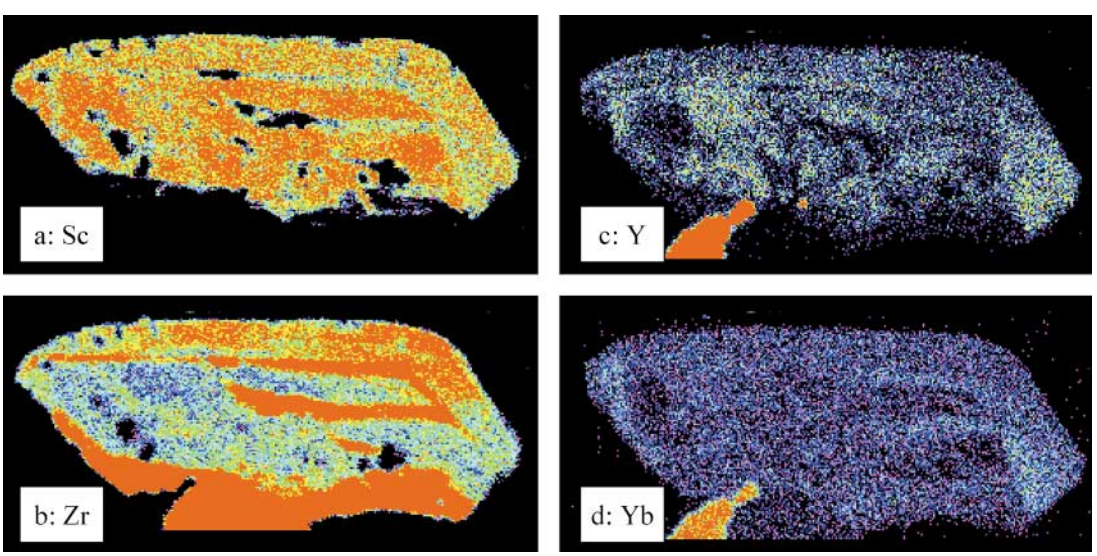

FIG. 5. Chemical zoning of a section of a pretulite crystal (see also Fig. 3), observed with EPMA elemental mapping (a to d: Sc, Zr, Y and Yb, respectively). Colors range from violet to red, and indicate an increasing concentration of the element. In a, red areas correspond to zone A of Figure 3; zone D (black) is not visible. In b, well-defined red areas correspond to Zr-rich parts of zone B (center) and to zone D (bottom, with zircon). Individual maps do not allow us to distinguish zone C.

TABLE 1. RESULTS OF ELECTRON-PROBE MICRO-ANALYSES OF PRETULITE FROM SAINT-AUBIN-DES-CHÂTEAUX

	Zone A							Zone B		Zone C					Zone D								Thin section								
	1	2	3	4	5	6	7	8	9	10	11	12	13	14	15	16	17	18	19	20	21	22	23	24	25	26	27	28	29	30
Sc_2O_3 wt.%	47.71	47.79	47.18	46.85	46.91	46.27	45.61	42.15	40.21	42.12	44.42	43.69	43.87	44.41	33.28	33.19	32.47	32.26	31.37	36.54	33.87	32.37	33.26	31.90	31.68	32.10	30.63	28.42	29.43	18.58
Y_2O_3	1.33	1.46	1.36	1.77	1.24	2.36	2.96	2.74	1.85	4.34	3.14	3.19	2.74	2.10	1.09	1.41	0.99	0.99	0.99	1.35	1.25	1.17	0.70	0.54	0.89	0.72	0.51	0.79	0.93	1.51
Yb_2O_3	0.28	0.49	0.43	1.07	0.88	0.46	0.92	2.06	1.44	2.54	1.20	1.48	1.26	1.09	0.74	0.90	0.91	0.89	0.77	1.06	0.53	0.87	0.99	0.48	-	-	0.55	-	0.69	1.35
Er_2O_3	0.17	0.18	0.18	0.25	0.32	0.43	0.47	0.51	0.39	0.82	0.53	0.56	0.45	0.32	0.23	0.19	0.21	0.27	0.21	-	0.36	-	-	-	-	-	-	-	-	0.56
Lu_2O_3	-	0.16	-	-	0.23	-	-	0.51	0.35	0.48	-	0.14	0.22	0.27	0.17	0.18	0.20	0.22	0.19	n.d.	n.d.	n.d.	n.d.	n.d.	n.d.	n.d.	n.d.	n.d.	n.d.	n.d.
Dy_2O_3	-	0.15	-	-	-	0.20	-	-	-	0.30	0.24	0.17	0.17	-	-	-	-	-	0.18	0.54	-	-	-	-	-	-	-	-	-	0.37
ZrO_2	0.61	0.53	0.34	0.41	0.66	0.50	0.55	3.45	6.93	0.43	1.61	2.00	2.27	2.78	17.28	17.81	18.52	19.10	19.99	11.33	17.07	19.30	19.91	20.22	20.29	21.52	21.46	24.85	25.38	36.71
HfO_2	-	-	-	-	-	-	-	-	-	-	-	-	-	-	0.29	0.21	0.22	0.21	0.33	0.38	0.25	0.47	0.35	0.19	0.33	0.29	0.33	0.49	0.28	0.54
P_2O_5	48.97	49.17	48.88	49.43	50.08	49.84	49.38	46.38	45.01	47.23	48.56	46.12	47.23	47.77	35.81	35.90	34.87	34.26	33.96	40.06	35.97	35.09	35.39	33.03	33.32	33.46	32.80	30.63	30.92	20.82
SiO_2	0.24	0.24	0.24	0.53	0.51	0.28	0.36	1.80	3.38	0.41	0.75	0.98	1.20	1.43	9.54	9.82	9.86	9.97	10.89	5.63	8.86	10.24	9.55	10.47	10.36	10.72	11.33	12.39	11.91	17.01
Al_2O_3	0.13	0.17	0.15	0.13	0.11	0.09	0.13	0.09	0.09	0.08	0.13	0.11	0.11	0.08	0.09	0.09	0.08	0.11	0.09	n.d.	n.d.	n.d.	n.d.	n.d.	n.d.	n.d.	n.d.	n.d.	n.d.	n.d.
FeO	-	-	-	-	-	-	-	-	-	-	-	-	-	-	-	-	-	-	-	0.41	0.47	0.56	0.04	0.48	0.41	0.45	0.45	0.72	0.53	0.58
Total	99.4	100.3	98.8	100.4	101.0	100.4	100.4	99.7	99.7	98.8	100.6	98.4	99.5	100.3	98.5	99.7	98.3	98.3	99.0	97.3	98.6	100.1	100.2	97.3	97.3	99.3	98.1	98.3	100.1	98.0
Sc *apfu*	0.983	0.979	0.979	0.961	0.958	0.951	0.942	0.896	0.858	0.906	0.924	0.933	0.924	0.925	0.740	0.731	0.727	0.725	0.702	0.808	0.748	0.710	0.730	0.718	0.713	0.710	0.688	0.644	0.659	0.452
Y	0.017	0.018	0.017	0.022	0.016	0.030	0.037	0.036	0.024	0.057	0.040	0.042	0.035	0.027	0.015	0.019	0.014	0.014	0.014	0.018	0.017	0.016	0.009	0.007	0.012	0.010	0.007	0.011	0.013	0.022
Yb	0.002	0.004	0.003	0.008	0.006	0.003	0.007	0.015	0.011	0.019	0.009	0.011	0.009	0.008	0.006	0.007	0.007	0.007	0.006	0.008	0.004	0.007	0.008	0.004	-	-	0.004	-	0.005	0.012
Er	0.001	0.001	0.001	0.002	0.002	0.003	0.003	0.004	0.003	0.006	0.004	0.004	0.003	0.002	0.002	0.002	0.002	0.002	0.002	-	0.003	-	-	-	-	-	-	-	-	0.005
Lu	-	0.001	-	-	0.002	-	-	0.004	0.003	0.004	-	0.001	0.002	0.002	0.001	0.001	0.002	0.002	0.001	n.d.	n.d.	n.d.	n.d.	n.d.	n.d.	n.d.	n.d.	n.d.	n.d.	n.d.
Dy	-	0.001	-	-	-	0.001	-	-	-	0.002	0.002	0.001	0.001	-	-	-	-	-	0.002	0.004	-	-	-	-	-	-	-	-	-	0.003
Zr	0.007	0.006	0.004	0.005	0.008	0.006	0.006	0.041	0.083	0.005	0.019	0.024	0.027	0.032	0.215	0.219	0.232	0.240	0.250	0.140	0.211	0.237	0.244	0.255	0.256	0.266	0.270	0.315	0.318	0.500
Hf	-	-	-	-	-	-	-	-	-	-	-	-	-	-	0.002	0.002	0.002	0.002	0.002	0.003	0.002	0.003	0.003	0.001	0.002	0.002	0.002	0.004	0.002	0.004
P	0.981	0.979	0.986	0.986	0.994	0.996	0.991	0.958	0.933	0.988	0.981	0.957	0.966	0.967	0.773	0.768	0.759	0.748	0.738	0.861	0.772	0.748	0.755	0.723	0.729	0.719	0.716	0.675	0.673	0.493
Si	0.006	0.006	0.006	0.013	0.012	0.007	0.009	0.044	0.083	0.010	0.018	0.024	0.029	0.034	0.243	0.248	0.254	0.257	0.280	0.149	0.234	0.268	0.250	0.282	0.279	0.283	0.304	0.336	0.319	0.495
Al	0.004	0.005	0.004	0.004	0.003	0.003	0.004	0.003	0.003	0.002	0.004	0.003	0.003	0.002	0.003	0.003	0.002	0.003	0.003	n.d.	n.d.	n.d.	n.d.	n.d.	n.d.	n.d	n.d.	n.d.	n.d.	n.d.
Fe	-	-	-	-	-	-	-	-	-	-	-	-	-	-	-	-	-	-	-	0.009	0.010	0.012	0.001	0.010	0.009	0.010	0.010	0.016	0.011	0.014

A, B, C and D: different zones of the crystal shown in Figures 3 and 5; other datasets pertain to the (Zr,Si)-rich rim of pretulite crystals from a thin section (Fig. 4). Analytical conditions: Cameca microprobe SX 50 (BRGM – CNRS – University common laboratory, Orléans); voltage 20 kV; intensity 20 nA; standards: synthetic pure phosphates (Y, Yb, Er, Lu and Dy $L\alpha$), synthetic zircon (Zr$L\alpha$), synthetic hafnium oxide (Hf$L\alpha$), synthetic pretulite (Sc$K\alpha$ and P$K\alpha$), albite (Si$K\alpha$), synthetic corundum (Al$K\alpha$), hematite (Fe$K\alpha$); detection limit of the elements (wt.%): Al, Si 0.015, P 0.02, Ca 0.03, Fe, Sc 0.05, Hf 0.07, Zr 0.09, Y 0.10, REE 0.11, Th 0.20; - : below detection limit; n.d.: not determined.

Yb, then Er, Dy and Lu, with a total below 1.3 wt.% of the respective oxides); zirconium and silicon contents are very low, below 0.6 wt.% ZrO_2 and 0.4% SiO_2. The composition richest in Sc (no. 1) corresponds to the formula: $[Sc_{0.983}(Y_{0.017}Yb_{0.002}Er_{0.001})_{\Sigma 0.020}Zr_{0.007}](P_{0.981}Si_{0.006}Al_{0.004})O_{3.989}$, simplified as $Prt_{0.973}Xnt_{0.020}Zrn_{0.007}$. In the B zone (nos. 8–9), the pretulite shows a significant enrichment in Zr and Si, up to 6.9 wt.% ZrO_2 and 3.4% SiO_2. Composition 9 corresponds to $[Sc_{0.858}(Y_{0.024}Yb_{0.011}Er_{0.003}Lu_{0.003})_{\Sigma 0.041}Zr_{0.083}](P_{0.933}Si_{0.083}Al_{0.003})O_{4.018}$, or $Prt_{0.873}Xnt_{0.042}Zrn_{0.085}$.

In the C zone (nos. 10–14), the pretulite shows minor amounts of Zr and Si (below 2.8% ZrO_2 and 1.4% SiO_2), with an enrichment in Y (up to 4.3% Y_2O_3) and *HREE* (especially Yb, up to 2.5% Yb_2O_3). The composition richest in (Y,*HREE*), no. 10, corresponds to $[Sc_{0.906}(Y_{0.057}Yb_{0.019}Er_{0.006}Lu_{0.004}Dy_{0.002})_{\Sigma 0.088}Zr_{0.005}](P_{0.988}Si_{0.010}Al_{0.002})O_{3.994}$, or $Prt_{0.907}Xnt_{0.088}Zrn_{0.005}$. In the D zone (nos. 15–19), the pretulite reveals high Zr and Si contents (17–20% ZrO_2 and 9–11% SiO_2); minor quantities of Y and Yb are present in similar proportions (about 1 wt.% of the respective oxides). Composition 19 corresponds to $[Sc_{0.702}(Y_{0.014}Yb_{0.006}Er_{0.002}Lu_{0.001}Dy_{0.002})_{\Sigma 0.023}Zr_{0.250}Hf_{0.002}](P_{0.738}Si_{0.280}Al_{0.003})O_{3.997}$, or $Prt_{0.718}Xnt_{0.024}Zrn_{0.258}$.

In all cases enriched in Zr and Si (over 0.02 atoms per formula unit, *apfu*), the atomic ratio Zr/Si is invariably close to 1, in agreement with a solid-solution scheme according to the coupled heterovalent substitution $Sc^{3+} + P^{5+} \leftrightarrow Zr^{4+} + Si^{4+}$; the molar ratio $ScPO_4/ZrSiO_4$ attains 2.8. Electron-microprobe data on pretulite from a thin section confirm these results. In the areas with the higher Zr and Si contents, in the D zone (Table 1, nos. 20–30), the molar ratio $ScPO_4/ZrSiO_4$ generally varies between 3.5 and 2.1, but was found to be as low as 0.90 for one composition (no. 30), thus corresponding to a scandian zircon with formula $[Sc_{0.452}(Y_{0.022}Yb_{0.012}Er_{0.005}Dy_{0.003})_{\Sigma 0.042}Zr_{0.500}Hf_{0.004}](P_{0.493}Si_{0.495}Fe_{0.014})O_{4.000}$, or $Prt_{0.453}Xnt_{0.042}Zrn_{0.505}$.

The pretulite from Saint-Aubin is much richer in Y and *HREE* (Yb, Er and Dy, and Lu) than the sample from Höllkogel, the type locality (Bernhard *et al.* 1998b). It is also distinguished by its complex growth-induced zoning, and by the development of compositions intermediate between ideal pretulite and zircon.

Crystallography

Despite its relatively large size, the pretulite crystal shown in Figure 2 was used for a single-crystal X-ray study, with an imaging plate system. Operating conditions and related data are given in Table 2. On the basis of its tetragonal symmetry, the unit-cell parameters of the Saint-Aubin material are *a* 6.5870(9), *c* 5.809(1) Å. Table 3 and Figure 6 compare these new data with those of pretulite from the type locality, pure synthetic $ScPO_4$, and related isotypic compounds (synthetic YPO_4, zircon and various *HREE* phosphates).

Diffraction data were used to solve the average structure of this sample of pretulite. Table 4 gives the coordinates of the atoms in the unit cell. Owing to its complex chemical composition, the structure was refined by 1) adjusting the Sc/Zr value, and, accordingly, the P/Si value, and 2) adjusting the Sc/(Y,*HREE*) value, considering all heavy rare-earth elements (*HREE*) as Yb, with Sc/Y and Yb/Y values close to the mean of Sc/Y and *HREE*/Y values indicated by the electron-microprobe data (Table 1). The best *R* value (0.039) was thus obtained for the simplified structural formula $[Sc_{0.904}Y_{0.032}(Yb,HREE)_{0.016}Zr_{0.048}](P_{0.952}Si_{0.048})O_4$, close to a composition of the C zone. This solution represents an average structure of a relatively inhomogeneous crystal, which explains the lower accuracy of these data compared to those of Bernhard *et al.* (1998b) ($R = 0.019$) for the Austrian pretulite. Nevertheless, the relatively low *R* value, as well as the homogeneity of *U* factors, indicate that this solution is a good approximation of the real structure. A listing of observed and calculated structure-factors is available from the Depository of Unpublished Data, CISTI, National Research Council, Ottawa, Ontario K1A 0S2, Canada.

According to Table 3, the *a* and *c* parameters increase in going from pure synthetic $ScPO_4$ to the pretulite from Saint-Aubin owing to the substitution of larger cations, Y and *HREE*, for Sc, as well as to the presence of the zircon component. The two natural examples of pretulite have very close unit-cell volumes, but a higher density (3.83 g/cm^3) was calculated for the Saint-Aubin material owing to its enrichment in the heavier elements.

TABLE 2. DATA ON THE CRYSTAL OF PRETULITE FROM SAINT-AUBIN-DES-CHÂTEAUX CHOSEN FOR STRUCTURE REFINEMENT, AND EXPERIMENTAL DETAILS

Crystal data

Simplified structural formula		$(Sc_{0.904}Y_{0.032}Yb_{0.016}Zr_{0.048})(P_{0.952}Si_{0.048})O_4$	
Crystal system: tetragonal		Space group: *I*4$_1$/*amd* (# 141)	
a	6.5870(9) Å	*c*	5.809(1) Å
V	252.05(7) Å^3	*Z*	4
Density	3.834 g/cm^3 (calculated)	Absorption coefficient: 4.56 mm^{-1}	

Data Collection

Temperature: ambient	Crystal size: 200 × 160 × 110 μm
Radiation: MoKα (λ = 0.71073 Å)	50 kV, 40 mA
Diffractometer: STOE IPDS single φ axis	Method: imaging plate technology
φ range: 0-201°	Δφ (increment): 3°
Crystal-to-detector distance (IP)	60 mm
Irradiation time per exposure	5 minutes
θ range: 1.9 to 28.2°	Reflections collected: 1060
Independent reflections: 90	[R(int) = 0.0802]
Reflections with I > 2σ(I): 84	
Index ranges: $-8 \le h \le 8, -8 \le k \le 8, -7 \le l \le 7$	

Refinement

Refinement method: Full-matrix least-squares on F^2	
Data/restraints/parameters: 90/0/12	Goodness-of-fit on F^2: 2.466
R1 [I > 2σ(I)]: 0.0389	ωR2: 0.1407
R index (all data): 0.0408	ωR2: 0.1412
Largest diff. peak/hole: 0.598, -0.729 e.Å^{-3}	

TABLE 3. VARIATION OF THE UNIT-CELL PARAMETERS OF NATURAL AND SYNTHETIC *REE* PHOSPHATES WITH THE ZIRCON STRUCTURE-TYPE

Compound	*a* (Å)	*c* (Å)	*V* (Å³)	D (g/cm³)	*c*/*a*	Reference
Zircon (synthetic)	6.605	5.982	261.0	4.67	0.906	Siggel & Jansen (1990)
Zircon	6.612	5.994	262.0	(4.69)*	0.907	Finger (1974)
$ScPO_4$ (synthretic)	6.574	5.791	250.3	3.71	0.881	Milligan *et al.* (1982)
$ScPO_4$ (synthetic)	6.578	5.796	250.8	3.71	0.881	Rasmussen *et al.* (1993)
$(Sc,Y)PO_4$ Pretulite	6.589	5.806	252.1	3.71	0.881	Bernhard *et al.* (1998b)
$[(Sc,Y,Yb),Zr](P,Si)O_4$	6.587	5.809	252.1	3.83	0.882	this study (Table 2)
$LuPO_4$ (synthetic)	6.783	5.947	273.6	6.55	0.877	Ni *et al.* (1995)
$YbPO_4$ (synthetic)	6.809	5.964	276.5	6.40	0.876	Ni *et al.* (1995)
$YbPO_4$ (synthetic)	6.816	5.966	277.2	6.40	0.875	Milligan & Mullica (1983)
$TmPO_4$ (synthetic)	6.829	5.980	278.9	6.29	0.876	Ni *et al.* (1995)
$ErPO_4$ (synthetic)	6.851	5.997	281.4	6.19	0.875	Ni *et al.* (1995)
$HoPO_4$ (synthetic)	6.877	6.018	284.6	6.07	0.875	Ni *et al.* (1995)
YPO_4 (synthetic)	6.882	6.018	285.0	4.25	0.874	Milligan *et al.* (1982)
Xenotime-(Y)	6.895	6.028	286.5	4.68**	0.874	Ni *et al.* (1995)
Xenotime-(Yb)	6.866	6.004	283.0	5.85***	0.874	Buck *et al.* (1999)
$DyPO_4$ (synthetic)	6.905	6.038	287.9	5.94	0.874	Ni *et al.* (1995)
$TbPO_4$ (synthetic)	6.931	6.061	291.1	5.79	0.874	Ni *et al.* (1995)

* Natural zircon with unknown Hf content; *d* calculated on the basis of hypothetical Hf/Zr = 2% (atomic).
** Also with *HREE* and Ca. *** Also with Y and *HREE*.

TABLE 4. ATOM COORDINATES IN THE STRUCTURE OF PRETULITE FROM SAINT-AUBIN-DES-CHÂTEAUX, FRANCE

	site	*x*	*y*	*z*	*U*(eq)	o. f.
Sc	4 *b*	½	¼	⅛	0.009(1)	0.904
Y	"	"	"	"	0.009(1)	0.032
Yb	"	"	"	"	0.009(1)	0.016
Zr	"	"	"	"	0.009(1)	0.048
P	4 *a*	½	¼	⅝	0.007(1)	0.952
Si	"	"	"	"	0.007(1)	0.048
O	16 *h*	0.1806(5)	¼	0.436(6)	0.009(1)	1

The equivalent isotropic displacement parameters *U*(eq) (in Å²) is defined as one third of the orthogonalized U^{ij} tensor. o.f.: occupancy factor.

Raman spectroscopy

The Raman spectrum of pretulite is presented for the first time; it was obtained on the largest crystal shown in Figure 4, as well as on a sample (HK1A) from the type locality, provided by F. Bernhard. As the presence of *REE* in pretulite induces strong fluorescence lines, pure synthetic $ScPO_4$ (provided by Eugene Jarosewich), used as Sc standard for the electron-probe micro-analyses, also was studied for comparison. Data were obtained with a DILOR XY800 Raman microprobe (BRGM – CNRS – Université d'Orléans, Dr. J.-M. Bény, ISTO–CNRS, Orléans, analyst). Operating conditions were: Ar^+ laser, λ of the exciting radiations 488 and 514.5 nm, 25 mW (~3 mW on the sample), recording window 60–2020 cm^{-1}, objective ×100, and acquisition time 120 s.

The spectra obtained on pretulite from Saint-Aubin with the two laser sources allow us to distinguish complex groups of strong *REE*-fluorescence-induced bands from fine specific Raman bands (Fig. 7a). A comparison of the Raman spectrum of pretulite from the type locality with that of *REE*-free synthetic $ScPO_4$ (Fig. 7b) confirms the discrimination between fluorescence and Raman bands. All three samples present eleven well-defined Raman bands (Raman shift in cm^{-1}): a very strong pair at 1079–1082 and 1024–1026, with an intermediate doublet at 1049–1053 and 1043–1045, then seven medium to weak bands at 595, 474–475, 331–334, 326, 240–243, 234 and 186–187. This Raman spectrum is similar to that obtained for xenotime-(Y) (C. Bény, unpubl. data), but with an increase of about 30 cm^{-1} of the Raman shift of the two strongest bands.

SCANDIAN ZIRCON

Zoned detrital zircon

The finely stratified ironstone shows numerous detrital crystals of zircon, generally with titanium oxides in peculiar millimetric layers. In reflected light and SEM–BSE images, these zircon crystals commonly display concentric zoning (Fig. 8) indicative of a primary oscillatory growth. The usually anhedral to subhedral morphology of the zircon crystals, which cuts this growth zoning, clearly indicates their detrital origin, without recrystallization. This kind of zircon was described in iron ores of Lower Ordovician age by Chauvel (1968, 1974), as well as in rutile- and zircon-rich sandstones from the Armorican Massif by Faure (1978).

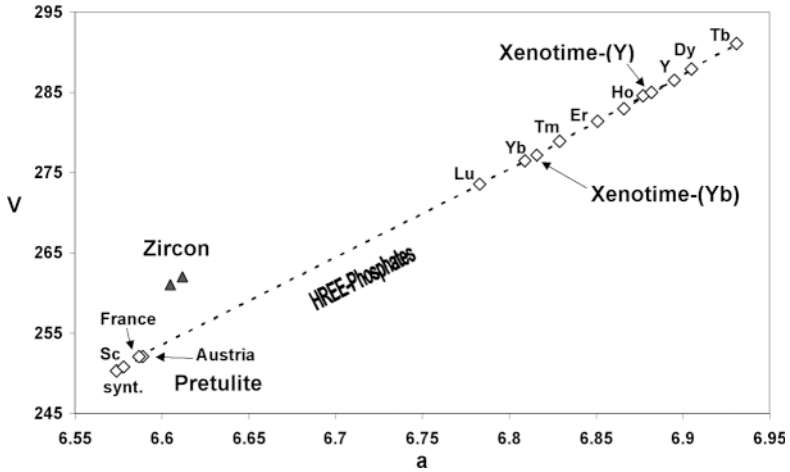

FIG. 6. Variation of the unit cell parameters a (Å) and V (Å^3) within the series of *HREE* phosphates related to the zircon structure-type, compared to that of zircon (according to data of Table 3).

Nevertheless, in the A horizon at Saint-Aubin, the proportion of such zoned crystals (about one third) is particularly high.

Results of the electron-probe micro-analyses are given in Table 5. The dark zones correspond to a phosphate enrichment, together with Sc, Y, Yb, Er, Fe, Ca and Al (and, in some cases, Lu and Th; U is below detection limit). These dark zones give low analytical totals, from 95 down to 92 wt.%, whereas the light zones (pure zircon) give totals close to 100 wt.%. Such a deficit is not strictly correlated with the cumulative sum of P and associated cations, and could not be explained by the omission of less abundant *HREE*, or *LREE* in the analytical process. It reveals a metamict state of these zones, enriched in H_2O (maximum ~5–8 wt.%). It is well known that there is a positive correlation among Y, U and P in zircon (see, for instance, Köppel & Sommerauer 1974), which explains the indirect correlation observed between Y (and the *REE*) and the metamictization process (Larsen *et al.* 1953).

An increasing P content is correlated positively with the amount of *HREE*, Y and Sc (but negatively with Fe, at high P contents). The level of scandium reaches 3.18 wt.% Sc_2O_3 for the composition richest in P (8.2 wt.% P_2O_5), which corresponds to the formula (without H_2O): $Zr_{0.76}Hf_{0.01}[Sc_{0.09}Y_{0.07}(HREE)_{0.03}]_{\Sigma 0.19}Al_{0.03}Fe_{0.03}Ca_{0.02}(Si_{0.75}P_{0.22})_{\Sigma 0.97}O_{4.02}$. In the light zones, P, Sc, Ca and Al are below detection limits, and *HREE* and Fe decrease significantly; only hafnium is systematically present (0.8 to 2.3 wt.% HfO_2), as in all crystals.

According to Geisler & Schleicher (2000) and Geisler *et al.* (2001), a significant Ca content (>0.2 wt.% CaO) in the metamict zones of zircon is indicative of hydrothermal leaching or of weathering, which introduces Ca (and probably Fe, Al and Mn), with a loss of Zr, Si and radiogenic Pb (possibly U also). In contrast, at Saint-Aubin, Y, Sc and the *HREE* are clearly primary, to counterbalance the phosphate anion, and the zoning of zircon indicates an oscillatory growth between end-member zircon and a phosphate-type component [a mixture of pretulite and xenotime-(Y)].

Except for scandium, all minor elements detected in the zoned crystals are commonly found in natural zircon (Deer *et al.* 1997). An analysis for scandium is generally omitted in analytical work on zircon. However, this element may commonly be present as a minor component together with Y and *HREE* in phosphorus-rich varieties of this mineral. Among others, Romans *et al.* (1975) have demonstrated that scandium is systematically present, with a mean content of 0.2 wt.%, in the magnetic fraction of zircon enriched in Y and P from three commercial concentrates, with a maximum of 0.7 wt.% Sc in a zoned crystal (together with 7.5% Y and 4.1% P). Zircon with about 1 wt.% Sc_2O_3 has been discovered at Baveno (Italy) by Gramaccioli *et al.* (2000). Another example is an exotic occurrence of a "solid solution of zircon and xenotime-(Y)" described recently by Mordberg *et al.* (2001) in the Schugorsk bauxite deposit, in Russia. This phase crystallized during bauxite weathering at the contact between zircon and xenotime grains. Chemically, it corresponds to zircon with up to 5.8 wt.% Y_2O_3, and 3.3% Sc_2O_3 (and up to 3.8% P_2O_5), but the level of the HREE was apparently not established (total below 92 wt.%). This composition is very close to that of the zones richest in P in the detrital zircon from Saint-Aubin.

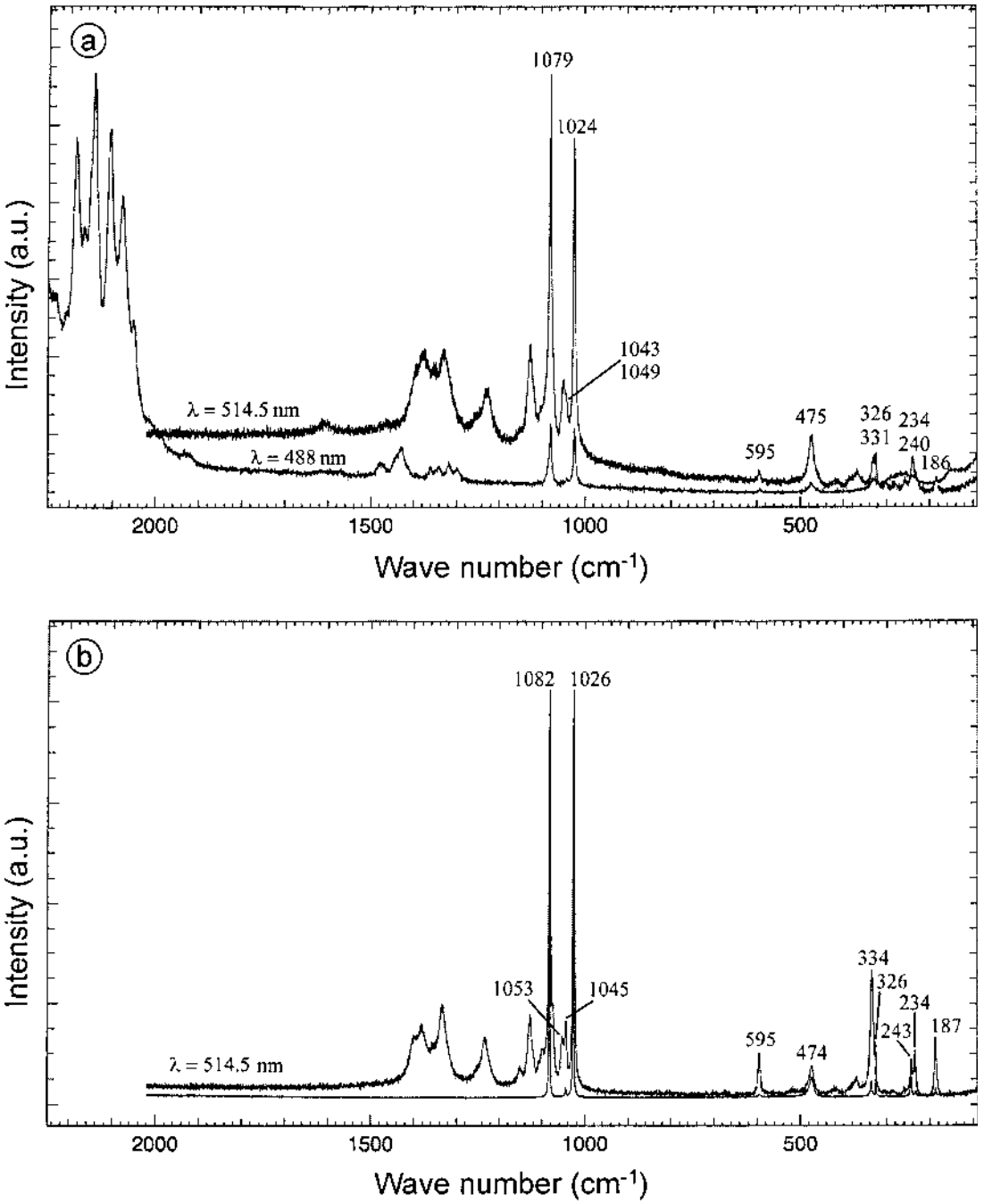

FIG. 7. Raman spectra of natural and synthetic pretulite. (a) (top): two spectra of pretulite from Saint-Aubin-des-Châteaux with two laser sources (λ = 488 and 514.5 nm); non-indexed lines are *REE* fluorescence bands. (b) (bottom): spectra at λ = 514.5 nm for pretulite from the type locality (Höllkogel, Austria), and for synthetic $ScPO_4$ (fluorescence bands absent). Intensity scale bar in arbitrary units.

TABLE 5. COMPOSITION OF DETRITAL ZIRCON COEXISTING WITH PRETULITE FROM SAINT-AUBIN-DES-CHÂTEAUX, FRANCE

No.	1	2	3	4	5	6	7	8	9	10	11
ZrO_2	49.46	53.69	55.88	56.97	63.85	63.65	64.57	64.47	64.13	65.21	64.23
HfO_2	1.00	1.48	1.36	0.98	1.00	1.40	1.10	0.93	2.32	0.92	0.84
SiO_2	23.83	25.20	25.76	26.64	32.75	32.67	33.30	33.08	33.13	32.83	32.78
P_2O_5	8.16	5.36	3.49	2.93	0.54	0.45	0.41	0.39	0.37	0.37	0.36
Sc_2O_3	3.18	1.66	1.11	0.77	-	-	-	-	-	-	-
Y_2O_3	4.40	2.71	1.11	1.31	0.66	0.16	-	-	-	-	-
Yb_2O_3	1.65	0.51	0.27	0.41	0.34	0.18	-	-	-	-	-
Er_2O_3	0.78	0.56	0.35	0.21	0.21	-	-	-	-	-	-
Lu_2O_3	0.25	-	-	-	-	-	-	-	-	-	-
Gd_2O_3	-	0.41	-	-	-	-	-	-	-	-	-
FeO	1.09	1.23	1.37	1.54	0.63	1.00	-	-	0.56	-	-
CaO	0.64	1.07	1.07	0.92	-	-	-	-	-	-	-
Al_2O_3	0.86	0.31	0.22	0.23	-	-	-	-	-	-	-
ThO_2	-	-	-	0.83	-	-	-	-	-	-	-
total	95.31	94.19	91.99	93.74	99.98	99.51	99.37	98.87	100.50	99.33	98.22
H_2O^*	4.69	5.81	8.01	6.26							

No.	1	2	3	4	5	6	7	8	9	10	11
Zr	0.757	0.841	0.898	0.904	0.948	0.948	0.962	0.965	0.950	0.975	0.969
Hf	0.009	0.014	0.013	0.009	0.009	0.012	0.010	0.008	0.020	0.008	0.007
Si	0.748	0.810	0.849	0.867	0.997	0.998	1.018	1.016	1.006	1.007	1.014
P	0.217	0.146	0.098	0.081	0.014	0.012	0.010	0.010	0.009	0.010	0.009
Sc	0.087	0.046	0.032	0.022	-	-	-	-	-	-	-
Y	0.073	0.046	0.019	0.023	0.011	0.003	-	-	-	-	-
Yb	0.016	0.005	0.003	0.004	0.003	0.002	-	-	-	-	-
Er	0.008	0.006	0.004	0.002	0.002	-	-	-	-	-	-
Lu	0.002	-	-	-	-	-	-	-	-	-	-
Gd	-	0.004	-	-	-	-	-	-	-	-	-
Fe	0.029	0.033	0.038	0.042	0.016	0.026	-	-	0.014	-	-
Ca	0.022	0.037	0.038	0.032	-	-	-	-	-	-	-
Al	0.032	0.012	0.009	0.009	-	-	-	-	-	-	-
Th	-	-	-	0.006	-	-	-	-	-	-	-

Phosphorus-rich compositions (columns 1 to 4) correspond to dark growth-zones, as in Figures 8 and 10. Columns 7, 8, 10 and 11 correspond to the zircon crystal shown in Figure 3. Analytical conditions: see Table 1. Additional standards: synthetic Gd phosphate (Gd$L\alpha$), Durango apatite (Ca K_α), synthetic thorianite (Th$M\alpha$). - : below detection limit. H_2O^*: maximum content in metamict zones, assuming a total of 100 wt.%. Compositions are expressed in weight % on the left, and in terms of cation proportions on the right (cation total = 2 atoms).

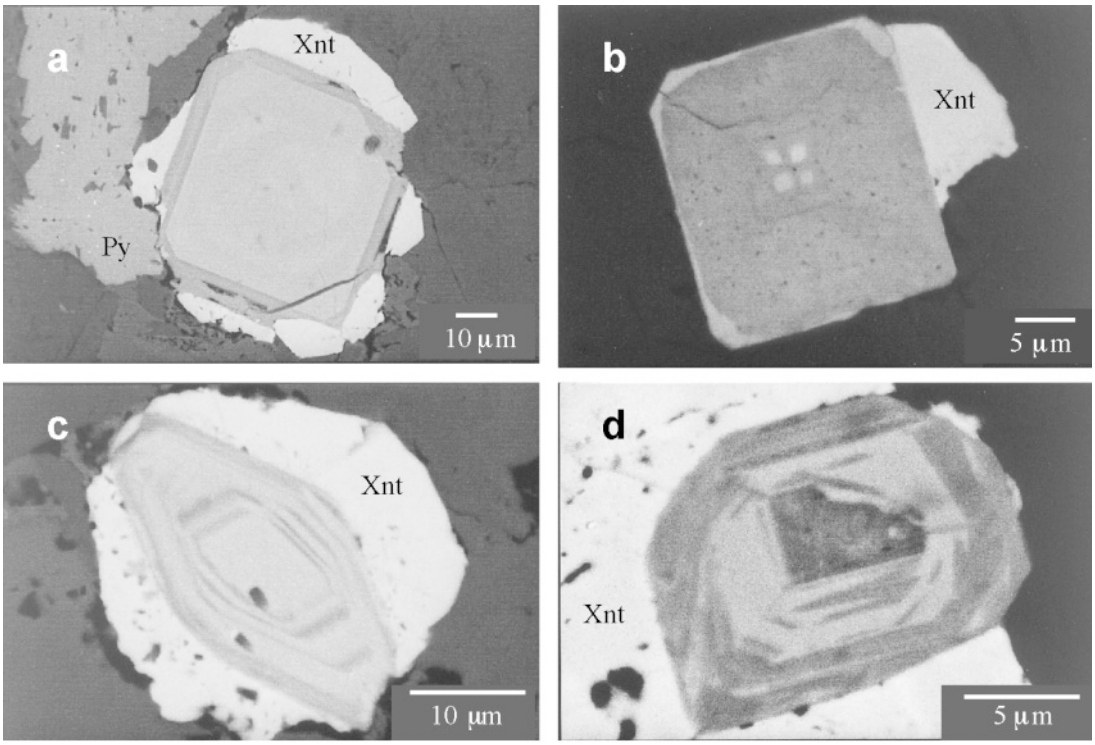

FIG. 8. Growth zoning of detrital zircon crystals (SEM–BSE images). (a) Square section with major pure zircon (light grey) with a rim of phosphate-rich variety (grey); white: xenotime-(Y) (Xnt in all images); grey area at left is pyrite (Py). (b) Dominant phosphate-rich zircon (grey) with a rim of normal variety (also at the center as four sector-growth zones). (c) Oblique section of a zircon crystal (light grey) with rhythmic zoning of phosphate-rich zones (grey). (d) Complex zoned crystal with a phosphate-rich center (grey-black), normal zircon (intermediate, light grey) and a phosphate-rich rim.

Neoformation of a zircon-type compound with an unusual composition

A systematic SEM–BSE examination of one thin section revealed the sporadic development of a microcrystalline rim around some crystals of zircon. Such a rim may appear on one side of the crystal, with an oscillatory development (Fig. 9a), or all around the detrital core (Fig. 9b). In some cases, the overgrowth seems to replace an initial volume of zircon, *i.e.*, as a result of a solution-and-redeposition process. According to Ewing (2001), such a local destabilization of zircon could be due to a leaching process under hydrothermal conditions.

A SEM–EDS analysis reveals a complex chemical composition, but the rim seems homogeneous in each case. In Figure 9a, the rim contains major amounts of Zr, Sc, Si and P, with minor Fe (4 wt.% Fe_2O_3), Y (2.5% Y_2O_3), Hf, Ca, Sr, Yb and U (approximately 1–1.5% of the respective oxides). The formula is: $(Zr_{0.49}Hf_{0.01})_{\Sigma 0.50}[Sc_{0.42}Y_{0.04}(HREE)_{0.01}]_{\Sigma 0.47}U_{0.08}Sr_{0.02}Fe_{0.10}Ca_{0.05}(Si_{0.51}P_{0.36})_{\Sigma 0.87}O_4$.

The rim shown in Figure 9b contains major amounts of Zr and Si (35% ZrO_2 and 17% SiO_2, mean result of three spot analyses), along with (wt.% of the respective oxides): Fe 5.7, P 8.0, Y 4.3, Sc 4.3, Ca 2.2, U 1.8, Sr 1.6 and Hf 1.5. Not considering Fe, Ca, Sr and U, this composition is close to 70% $ZrSiO_4$, 20% $ScPO_4$ and 10% YPO_4. Like for the composition of the dark zones within detrital zircon, the totals are low (80 to 90 wt.%), probably owing to partial or complete metamictization (leading to a high H_2O content), but also reflecting the fine-grained texture of the rim.

SCANDIAN XENOTIME-(Y)

Detrital crystals of zircon very commonly show an epitactic overgrowth of anhedral to subhedral xenotime-(Y) crystals (Figs. 4, 8), as has been observed in other deposits (*i.e.*, Petersen & Secher 1993). Such an over-

growth is generally related to hydrothermal processes, but a diagenetic formation also is possible (Fletcher *et al.* 2000, Cabella *et al.* 2001).

Figure 10 presents another well-developed example, where a zoned crystal of zircon is nearly completely surrounded by xenotime-(Y). The inner zone of xenotime-(Y) (Xnt2a), at the contact with zircon, presents a porous texture ("poikilitic crystallization"), whereas an outer zone (Xnt2b) has virtually no pores. A third zone (Xnt2c) is visible as a very fine light rim (less than 2 μm thick). Such a zoning has been observed in various crystals, and indicates multistage crystallization. Minute inclusions of galena have been observed in some cases in such overgrowths of xenotime-(Y).

Results of electron-probe micro-analyses of xenotime-(Y) are given in Table 6. Among the *REE*, holmium has been omitted, and some minor interferences involving *REE* emission lines (Roeder 1985) have been neglected. Nevertheless, it appears that the zoning of xenotime-(Y) is directly related to a decrease in the amount of Y, from the contact with zircon to the rim, together with a zonation in the distribution of the *REE*.

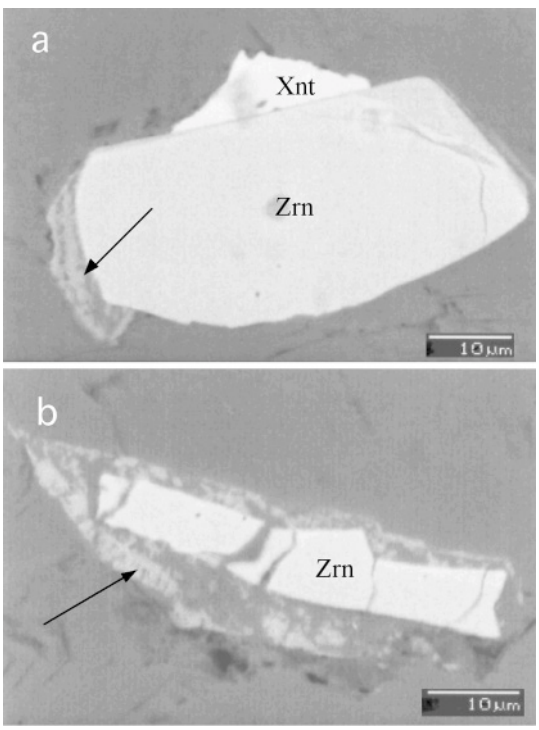

FIG. 9. a and b. SEM–BSE images of two examples of the late microcrystalline zircon-type rim (black arrow, composition between pretulite and zircon end-members) developed around detrital crystals of Sc-free zircon (Zrn). Xnt: xenotime-(Y).

In the first generation of xenotime-(Y), Xnt1 and Xnt3a have quite similar compositions, very close to that of Xnt2a (Xnt1, 2 and 3: distinct crystals). The major *REE* are Yb (7.0 to 7.3% Yb_2O_3), Er and Dy (up to 5.5 wt.% of the respective oxide), with minor Gd (less than 1.1% Gd_2O_3). The scandium content is around 0.2% Sc_2O_3. Iron, not detected in Xnt1, is over 1% Fe_2O_3 in Xnt2a.

In the second generation of xenotime-(Y), Xnt2b and Xnt3b show a marked increase of middle *REE* (Dy from 7.4 to 8.7% Dy_2O_3, Gd from 3.2 to 4.2% Gd_2O_3), with a corresponding depletion in Er and Yb (below 4.5% of the respective oxides). The Lu content is the same, Fe slightly increases, whereas Sc reaches 0.7% Sc_2O_3; this Sc maximum for Xnt2b corresponds to the formula $[Y_{0.678}(Dy_{0.080}Er_{0.046}Yb_{0.045}Gd_{0.035}Tb_{0.011}Lu_{0.006})_{\Sigma 0.223}Sc_{0.022}Fe_{0.047}Ca_{0.002}]_{\Sigma 0.972}P_{1.029}O_{4.055}$.

In the third generation of xenotime-(Y), the composition (Xnt2c) is close to that of Xnt2b, but with the addition of significant Sm and Eu contents (1.6% Sm_2O_3 and 0.8% Eu_2O_3). Uranium has been also detected (0.8% UO_2).

Scandium is invariably present, in the range 0.2–0.7 wt.% Sc_2O_3. Bernhard *et al.* (1998a) indicated a higher Sc content in uranium-rich xenotime-(Y) (1.9–2.7 wt. % Sc_2O_3) from Höllkogel, the type locality of pretulite.

Such a strong chemical contrast between generations of xenotime-(Y) at the crystal scale has rarely been documented. Sabourdy *et al.* (1997) indicated a similar enrichment in the middle *REE* Gd and Dy, and a corresponding decrease in Yb, from the center to the rim in alluvial crystals of xenotime-(Y) from the Limousin (Massif Central, France). They considered this zoning to be primary (magmatic). Bernhard *et al.* (1998a) presented SEM–BSE images of strongly zoned crystals of xenotime-(Y) from eastern Austria. At Saint-Aubin, there is a strong chemical discontinuity between zones of xenotime-(Y), as indicated also by the variation between zones *a* and *b* of the ratio of the middle to the heavy *REE* [(Gd + Dy) / (Er + Yb), Table 6] from 0.27 to 1.28 in Xnt2, and from 0.51 to 1.98 in Xnt3. Such a contrast necessarily reflects quite distinct thermochemical conditions of crystallization, acting at different paragenetic stages.

Solid Solutions Within the Ternary System $ScPO_4$ – (Y,*HREE*)PO_4 – $ZrSiO_4$

All our analytical data (SEM–EDS and EPMA) on pretulite, zircon and xenotime-(Y) have been plotted in terms of $ScPO_4$ – (Y,*HREE*)PO_4 – $ZrSiO_4$ (Fig. 11), together with data from the literature. Various compositions along (or close to) the zircon–pretulite join have been encountered, and further data would very probably fill the whole chemical spectrum between the two end-members. This plot thus suggests a continuous solid-solution between zircon and pretulite, corresponding to the heterovalent substitution $Zr^{4+} + Si^{4+} \leftrightarrow Sc^{3+} + P^{5+}$

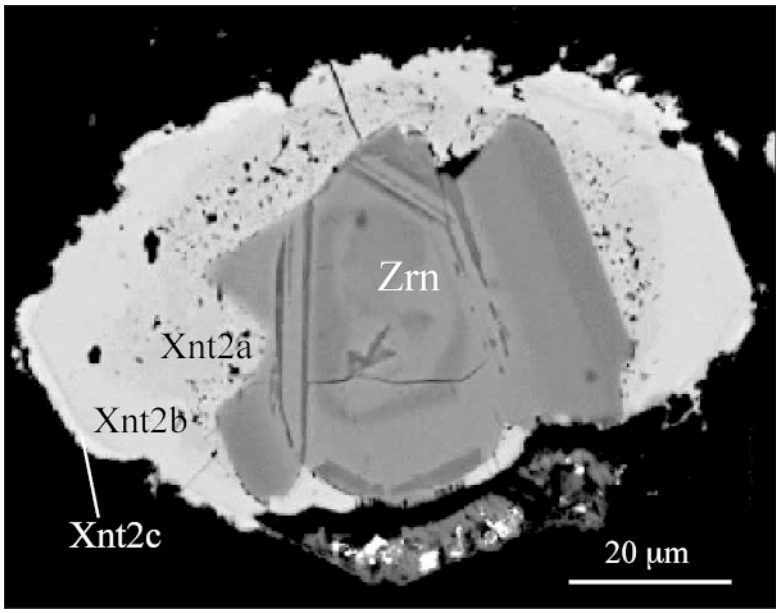

FIG. 10. Zoned crystal of zircon with an epitactic overgrowth of xenotime-(Y) (SEM–BSE image). Darkest growth-zones of zircon correspond to (Y,*REE*,Sc)- and P-enriched compositions. Xenotime-(Y) shows three distinct zones: inner zone Xnt2a (porous, light grey), outer zone Xnt2b (white grey), and fine rim Xnt2c (white).

TABLE 6. ELECTRON-MICROPROBE DATA ON XENOTIME-(Y) FROM SAINT-AUBIN-DES-CHÂTEAUX, FRANCE

	wt. % oxide							cation proportions (total = 2 atoms)					
	Xnt1	Xnt2a	Xnt2b	Xnt2c	Xnt3a	Xnt3b		Xnt1	Xnt2a	Xnt2b	Xnt2c	Xnt3a	Xnt3b
Anal.	3	2	2	1	4	2		3	2	2	1	4	2
Y_2O_3	40.1	40.7	38.0	33.8	41.3	39.0	Y	0.714	0.710	0.678	0.595	0.722	0.691
Sm_2O_3	-	-	-	1.6	-	-	Sm	-	-	-	0.018	-	-
Eu_2O_3	-	-	-	0.8	-	-	Eu	-	-	-	0.009	-	-
Gd_2O_3	0.8	0.3	3.2	3.9	1.1	4.2	Gd	0.009	0.003	0.035	0.042	0.011	0.046
Tb_2O_3	0.5	0.1	1.0	0.3	0.5	1.3	Tb	0.005	0.001	0.011	0.003	0.006	0.015
Dy_2O_3	5.3	3.0	7.4	5.6	5.0	8.7	Dy	0.057	0.031	0.080	0.059	0.053	0.093
Er_2O_3	5.5	5.5	4.3	4.2	5.4	4.0	Er	0.058	0.056	0.046	0.043	0.056	0.041
Tm_2O_3	0.8	0.9	-	-	0.8	-	Tm	0.008	0.009	-	-	0.008	-
Yb_2O_3	7.3	7.3	4.4	4.5	7.0	2.9	Yb	0.074	0.073	0.045	0.045	0.070	0.029
Lu_2O_3	0.9	0.8	0.6	0.5	0.9	0.6	Lu	0.009	0.008	0.006	0.005	0.009	0.006
Sc_2O_3	0.3	0.2	0.7	0.4	0.2	0.6	Sc	0.008	0.007	0.022	0.013	0.004	0.016
UO_2	-	-	-	0.8	-	-	U	-	-	-	0.006	-	-
CaO	0.1	0.5	0.1	0.3	0.1	0.1	Ca	0.005	0.016	0.002	0.010	0.004	0.004
FeO	0.0	1.3	1.7	2.3	0.4	0.7	Fe	0.000	0.037	0.047	0.063	0.011	0.019
P_2O_5	36.8	37.0	36.2	37.0	37.3	36.8	P	1.041	1.028	1.029	1.036	1.039	1.036
ZrO_2	0.2	0.9	-	0.4	0.1	-	Zr	0.003	0.014	-	0.006	0.002	-
SiO_2	0.3	0.2	-	0.7	0.2	0.1	Si	0.009	0.006	-	0.024	0.005	0.004
Al_2O_3	-	-	-	0.6	-	-	Al	-	-	-	0.022	-	-
							REE,Sc	0.228	0.189	0.244	0.237	0.217	0.246
Total	98.8	98.6	97.4	97.5*	100.2	98.9	R(M/H)	0.497	0.265	1.275	1.147	0.511	1.968

Xnt1: sample shown in Figure 3; Xnt2: sample shown in Figure 10 (a: inner porous zone; b: outer zone; c: white external rim); Xnt3: crystal from thin plate shown in Figure 4 (a: inner zone; b: outer zone) *REE*,Sc: total of *REE* + Sc. *R(M/H)*: atomic ratio between middle *REE* (Gd + Dy) and heavy *REE* (Er + Yb). *: excess of Fe, Si and Al due to chamosite inclusions. Analytical conditions: see Tables 1 and 5; elements programmed, not detected: La, Ce, Pr, Nd (Ho omitted), Sr, Th, Hf, Sr, S. Anal.: number of spot analyses. - : below detection limit.

(although one cannot totally exclude a syntactic intergrowth at a submicrometric scale). On the contrary, there is a large miscibility-gap between pretulite and xenotime-(Y), as shown initially by Bernhard *et al.* (1998a, b). Compositions of detrital zoned crystals of zircon give a linear trend, with an atomic ratio Sc/(Y,*HREE*) close to 1. Data on the zircon – xenotime-(Y) join are scarce; Deer *et al.* (1997) cited two cases of zircon from Japan with a (Y,*REE*) content close to 10 wt.% of the oxides, which corresponds to about 20 mol.% substitution. Romans *et al.* (1975) gave another example with about 25 mol.% substitution. These data are in accordance with the experimental study of Finch *et al.* (2001), which proved a wide miscibility-gap between zircon and xenotime-(Y).

The unit-cell volume of pretulite is closer to that of zircon than that of xenotime-(Y) (Table 3, Fig. 6): $V_{Ptl} = 250.6$, $V_{Zrc} = 261.0$, $V_{Xnt} = 286.5$ Å^3; $\delta V_{Ptl/Zrc} = -4.0\%$; $\delta V_{Xnt/Zrc} = +9.8\%$). These findings imply that the substitution $Sc^{3+} + P^{5+} \leftrightarrow Zr^{4+} + Si^{4+}$ should be easier than the substitution $(Y,HREE)^{3+} + P^{5+} \leftrightarrow Zr^{4+} + Si^{4+}$, which would favor an extensive solid-solution between zircon and pretulite.

In zircon, the simultaneous incorporation of Sc and (Y,*HREE*) will minimize the volume change, and thus enlarge the field of solid solution near the zircon end-member. This inference may explain the linear chemical trend observed in detrital zoned crystals of zircon.

Another geometric constraint is the variation of the ratio *c/a*, which decreases from zircon to pretulite [δ *c/a*) = –2.8%], then to xenotime-(Y) [δ *c/a*) = –3.5%]. Such a distortion factor may also favor the solid solution between pretulite and zircon. In any case, in a phosphorus-rich environment, the structure of zircon can better retain scandium in solid solution than yttrium or *HREE*. The scarcity of intermediate members in the continuous solid-solution series between zircon and pretulite, as well as in natural (Y,*HREE*)-rich zircon, thus probably is not due to crystal-chemical reasons, but rather to geochemical constraints, *i.e.*, probably the rarity of

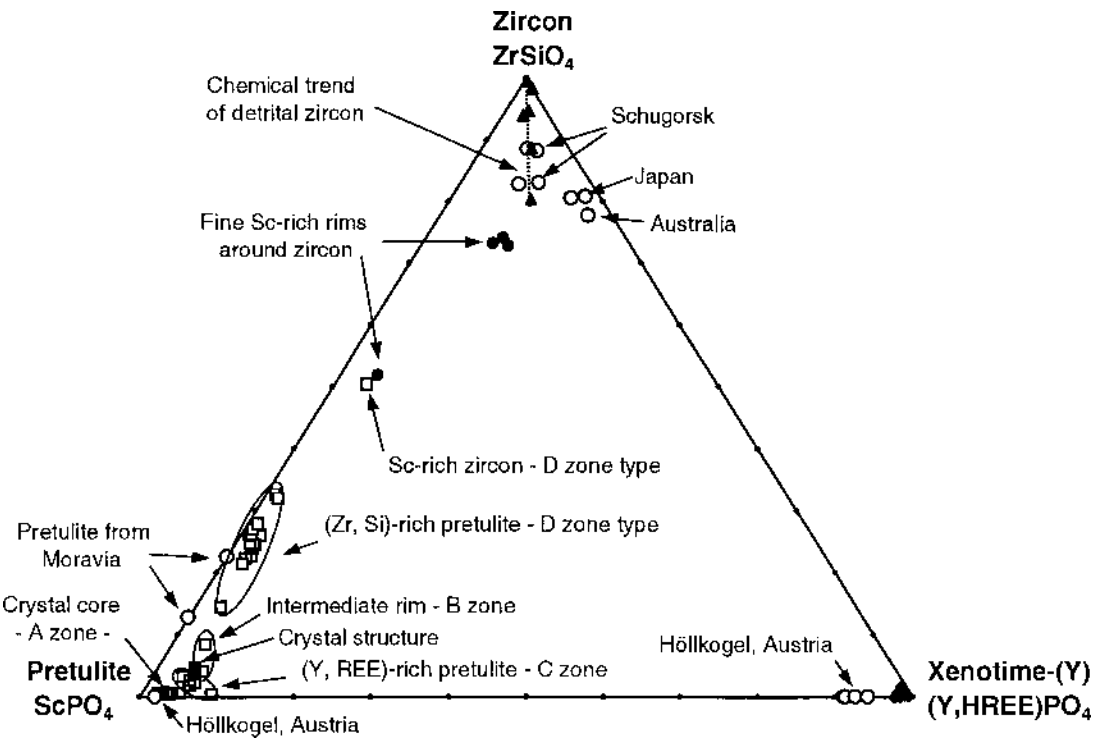

FIG. 11. Projection of the electron-microprobe data for pretulite, zircon and xenotime-(Y) from Saint-Aubin in the $ScPO_4$ – (Y,*HREE*)PO_4 – $ZrSiO_4$ system, supplemented with data from the literature. Open squares: EPMA data of the four zones of pretulite (Fig. 5a, Table 1); full square: composition from the crystal-structure study; full triangles with associated tie-line: EPMA data for detrital zircon along a chemical trend; full circles: SEM–EDS data for Sc-rich rim around zircon; full lozenges: xenotime-(Y). For comparison (open circles): pretulite and xenotime-(Y) from Höllkogel, Austria (type locality: Bernhard *et al.* 1998a, b) and from Dolní Bory, Moravia (Novák & Srein 1989); Y- and *HREE*-rich zircon from Japan (Deer *et al.* 1997), Australia (Romans *et al.*1975), and Schugorsk, Russia (Mordberg *et al.* 2001).

coprecipitation of zircon with phosphates of (Y,*HREE*) or Sc, especially during magmatic processes.

The data of Table 3 also permit a better understanding of the epitaxy of pretulite and xenotime-(Y) on zircon. The *a* parameter of pretulite is very close to that of zircon, which will favor an epitaxy on the (001) plane, and its growth along [001]; it explains the nucleation of two crystals of pretulite at the opposite sides of the elongation (along the A4 axis) of the main crystal of zircon in Figure 4. This inference was also confirmed by a morphological examination with an SEM of another pretulite–zircon association. On the contrary, the *c* parameter of xenotime-(Y) is very close to that of zircon, which will favor an epitaxy on a crystallographic plane containing the [001] direction, *i.e.*, a (*hk*0) plane; the growth of xenotime-(Y) crystal will be favored perpendicular to the A4 axis, as is the case in Figure 4.

Genetic Model for Scandium-Bearing Minerals at Saint-Aubin

We propose the following genetic scheme for the formation of Sc-bearing minerals at Saint-Aubin.

The first scandium-bearing mineral is zoned detrital zircon. Pretulite appeared later, but scandium required to grow pretulite crystals [like Y for xenotime-(Y)] cannot be inherited from this primitive zircon. For instance, the large crystal of pretulite in Figure 3 crystallized over a crystal of Sc-free zircon. A diffuse pre-concentration of scandium in the ironstone of the A horizon is necessary; it could lodged in sedimentary phosphates, or in (Fe, Mg)-silicates.

In a second step, the diagenetic and very low-grade metamorphic evolution of the ironstone induced a recrystallization process. Precursor phosphates gave the first generation of Sr-rich fluorapatite, and the bulk of the *REE*, Y and Sc was released (from phosphates or silicates), giving the first generation of xenotime-(Y) as well as pretulite (A-zone type, with nearly end-member composition). The same process may be proposed for the crystallization of disseminated monazite-(Ce). On the basis of the composition of the chlorite, the temperature did not reach 400°C during this phase (Prof. J.-J. Chauvel, Université de Rennes, pers. commun.).

Hydrothermal processes induced by tectonic events led to the destabilization of this metamorphic association by percolation through the A horizon. The early crystallization of a second generation of fluorapatite, followed by the formation of lulzacite, a Sr–Al–Fe phosphate, in quartz–siderite veins, suggests the partial dissolution of primary fluorapatite, which caused a fraction of its lanthanides to be released. This step could explain the next generations of xenotime-(Y), enriched in lighter *REE* (Gd and Dy), and of pretulite (B- and C-type zones), enriched in Y and *HREE*. This scheme would also explain the Sc enrichment of the second generation of xenotime-(Y), the enrichment in Zr and Si of the last generation of pretulite (D-type zone), and the formation of mixed phases with various intermediate compositions between pretulite and zircon.

Conclusions

Saint-Aubin is the third geological area in which pretulite is found, after the Austrian type-locality (Bernhard *et al.* 1998b), and the Dolní Bory pegmatites, in the Czech Republic (Novák & Srein 1989). It is also the third occurrence of scandium minerals in France, after the recent discovery of bazzite in the La Lauzière Massif, Savoie, French Alps by N. Meisser (De Ascencao Guedes & Valverde 2000), and thortveitite in the talc deposit of Trimouns, Ariège, Pyrénées (P. de Parseval, pers. commun.).

Sc-bearing minerals at Saint-Aubin reveal a complex geological and geochemical evolution, which is only partly understood. Whereas most occurrences of scandium minerals are linked to late hydrothermal processes generally related to felsic magmatism, the formation of pretulite at Saint-Aubin is quite unique, without any equivalent up to now. Whereas scandium is generally dispersed in rocks, owing to its crystal-chemical similarity with Fe, Mg and Al, paradoxically, at Saint-Aubin, Sc-bearing minerals are found within an iron ore. Despite the high Fe content of the A horizon, scandium can thus be concentrated in specific Fe-free minerals at low-temperature conditions (supergene to hydrothermal), owing to its strong affinity with phosphate ions (Gramaccioli *et al.* 2000, Liferovich *et al.* 1998). Another interesting fact is the late formation of various intermediate compositions between zircon and pretulite, which suggests a complete solid-solution between these two end-members. Implicit in our reconstruction is a local mobility of zirconium in solution at a low temperature.

At Saint-Aubin, the ironstone is particularly enriched in fluorapatite. According to mineralogical and petrographic studies, as well as bulk-rock analyses (Chauvel & Phan 1965, Chauvel 1974), this phosphate appears ubiquitously in all iron ore deposits of the Martigné–Ferchaud Paleozoic syncline. In such phosphate-rich environments, one may thus expect the discovery of new occurrences of diagenetic and metamorphic xenotime-(Y) and pretulite. In fact, Chauvel (1968) described an overgrowth around detrital crystals of zircon in some samples: it may correspond to epitactic xenotime-(Y) (or pretulite ?), rather than to a new generation of zircon. More generally, the presence of these accessory minerals in phosphate-rich metasedimentary rocks, as exemplified by the recent description by Cabella *et al.* (2001) of authigenic xenotime-(Y) and monazite in pelitic metacherts from central Liguria, in Italy, hold much promise as an indicator of the geological evolution of sedimentary units.

Another interesting problem is the origin of the detrital scandian zircon at a regional scale. According to Chauvel (1974), the ironstone horizons within the lower

member of the Arenigian Grès armoricain Formation are related to the weathering and destruction of Cadomian uplands, which are mainly formed of granitic to granodioritic batholiths. These magmatic rocks could thus be the main source of scandian zircon.

The phosphate-rich sedimentary iron ore at Saint-Aubin-des-Châteaux constitutes a new type of occurrence of scandium-bearing minerals at low-temperature conditions. It opens a new field of investigations of the mineralogy, geochemistry and metallogeny of scandium.

Acknowledgements

The authors are grateful to Professor J.-C. Chauvel and Dr. J.-J. Peucat (Laboratoire de Géologie, Université de Rennes), for their scientific comments. F. Bernhard (TU Graz, Austria) kindly provided a sample of pretulite from the type deposit. We sincerely thank Dr. J.-P. Pierres, chief geologist (Hervé Company) together with the personnel of the quarry at Saint-Aubin-des-Châteaux, who facilitated our field work and sampling. The technical assistance of J.-M. Bény (ISTO–CNRS, Orléans), A. Barreau (Université de Nantes) and J. Breton (B.R.G.M., Orléans) is greatly appreciated. The manuscript was greatly improved by critical reviews and extensive improvement of the English by F. Bernhard, Ru Cheng Wang and R.F. Martin. The authors are also indebted to G. Raade (Geologisk Museum, Oslo), F. Fontan (Associate Editor, Toulouse) and B. Deniaux (CNRS, France). The work of one of us (E.G.) was carried out during a research course at the Muséum National d'Histoire Naturelle de Paris, with Professor M. Guiraud, director of the Mineralogical Laboratory, and Drs. P.-J. Chiappero, J.-P. Lorand and G.-C. Parodi.

References

Bernhard, F., Schitter, F. & Finger, F. (1998a): Zur Altersstellung der Lazulith-Guartz-Gänge im unterostalpinen Grobgneiskomplex der Nordoststeiermark und des südlichen Niederösterreich. *Mitt. naturwiss. Ver. Steiermark* **128**, 43-56.

_____, Walter, F., Ettinger, K., Taucher, J. & Mereiter, K. (1998b): Pretulite, $ScPO_4$, a new scandium mineral from the Styrian and Lower Austrian lazulite occurrences, Austria. *Am. Mineral.* **83**, 625-630.

Buck, H.M., Cooper, M.A., Černý, P., Grice, J.D. & Hawthorne, F.C. (1999): Xenotime-(Yb), $YbPO_4$, a new mineral from the Shatford Lake pegmatite group, southeastern Manitoba, Canada. *Can. Mineral.* **37**, 1303-1306.

Cabella, R., Lucchetti, G. & Marescotti, P. (2001): Authigenic monazite and xenotime from pelitic metacherts in pumpellyite–actinolite-facies conditions, Sestri–Voltaggio Zone, central Liguria, Italy. *Can. Mineral.* **39**, 717-727.

Chauvel, J.-J. (1968): *Contribution à l'étude des gisements de fer de l'Ordovicien inférieur de Bretagne*. Thèse de doctorat Dr. ès-Sci. Nat., Université de Rennes, Rennes, France.

_____ (1974): Les minerais de fer de l'Ordovicien inférieur du bassin de Bretagne-Anjou, France. *Sedimentology* **21**, 127-147.

_____ & Phan, Kieu Duong (1965): Présence d'apatite strontianifère dans le minerai de fer de l'Ordovicien inférieur de Bretagne. *C. R. Acad. Sci. Paris* **260**, 2855-2857.

De Ascencao Guedes, R. & Valverde, J. (2000): Béryllium. *In* Les minéraux du Massif de La Lauzière. *Le Règne Minéral*, *Spec. Vol.* **VI**, 52-55.

Deer, W.A., Howie, R.A. & Zussman, J. (1997): *Rock-Forming Minerals*. **1A**. *Orthosilicates* (2nd ed.). The Geological Society, London, U.K. (418-442).

Ewing, R.C. (2001): The design and evaluation of nuclear-waste forms: clues from mineralogy. *Can. Mineral.* **39**, 697-715.

Faure, P.-P. (1978): *Les grès à rutile et zircon du Massif Armoricain*. Thèse, Ecole Nat. Sup. Mines, Paris, France.

Finch, R.J., Hanchar, J.M., Hoskin, P.W.O. & Burns, P.C. (2001): Rare-earth elements in synthetic zircon. 2. A single-crystal X-ray study of xenotime substitution. *Am. Mineral.* **86**, 681-689.

Finger, L.W. (1974): Refinement of the crystal structure of zircon. *Carnegie Inst. Wash. Yearbook* **73**, 544-547.

Fletcher, I.R., Rasmussen, B. & McNaughton, N.J. (2000): SHRIMP U–Pb geochronology of authigenic xenotime and its potential for dating sedimentary basins. *Aust. J. Earth Sci.* **47**, 845-859.

Geisler, T. & Schleicher, H. (2000): Improved U – Th – total Pb dating of zircons by electron microprobe using a simple new background modeling procedure and Ca as a chemical criterion of fluid-induced U–Th–Pb discordance in zircon. *Chem. Geol.* **163**, 269-285.

_____, Ulonska, M., Schleicher, H., Pidgeon, R.T. & Van Bronswijk, W. (2001): Leaching and differential recrystallization of metamict zircon under experimental hydrothermal conditions. *Contrib. Mineral. Petrol.* **141**, 53-65.

Gloaguen, E. (2002): *Etude structurale et métallogénique du minerai de fer hydrothermalisé de la carrière de Saint-Aubin-des-Châteaux, Loire-Atlantique* (*France*). Rapport de recherches, Géosystèmes 2001–2002, Université d'Orléans, Orléans, France.

Gramaccioli, C.M., Diella, V. & Demartin, F. (2000): The formation of scandium minerals as an example of the role of complexes in the geochemistry of rare earths and HFS elements. *Eur. J. Mineral.* **12**, 795-808.

HERROUIN, Y., DADET, P., GUIGUES, J., LAVILLE, P. & TALBO, H. (1989): Notice explicative, Carte géologique de la France (1/50 000), feuille de Bain-de-Bretagne (388). BRGM, Orléans, France.

HEY, M.H., MILTON, C. & DWORNIK, E.J. (1982): Eggonite (kolbeckite, sterrettite), $ScPO_4 \bullet 2H_2O$. *Mineral. Mag.* **46**, 493-497.

KÖPPEL, V. & SOMMERAUER, J. (1974): Trace elements and the behaviour of the U–Pb system in inherited and newly formed zircons. *Contrib. Mineral. Petrol.* **43**, 71-82.

LARSEN, E.S., JR., WARING, C.L. & BERMAN, J. (1953): Zoned zircon from Oklahoma. *Am. Mineral.* **38**, 1118-1125.

LÉONE, P., PALVADEAU, P. & MOËLO, Y. (2000): Structure cristalline d'un nouveau phosphate de strontium naturel (lulzacite), $Sr_2Fe^{2+}(Fe^{2+},Mg)_2Al_4(PO_4)_4(OH)_{10}$. *C.R. Acad. Sc. Paris*, Sér. **II c**, **3**, 301-308.

LIFEROVICH, R.P., SUBBOTIN, V.V., PAKHOMOVSKY, YA.A. & LYALINA, M.F. (1998): A new type of scandium mineralization in phoscorites and carbonatites of the Kovdor Massif, Russia. *Can. Mineral.* **36**, 971-980.

_____, YAKOVENCHUK, V.N., PAKHOMOVSKII, YA.A., BOGDANOVA, A.N. & BRITVIN, S.N. (1997): Juoniite, a new mineral of scandium from calcite-dolomite carbonatites of the Kovdor massif. *Zap. Vser. Mineral. Obshchest.* **126**(4), 80-88 (in Russ.).

MELLINI, M., MERLINO, S., ORLANDI, P. & RINALDI, R. (1982): Cascandite and jervisite, two new scandium silicates from Baveno, Italy. *Am. Mineral.* **67**, 599-603.

MILLIGAN, W.O., MULLICA, D.F., BEALL, G.W. & BOATNER, L.A. (1983): Structures of $ErPO_4$, $TmPO_4$ and $YbPO_4$. *Acta Crystallogr.* **C39**, 23-24.

_____, _____, _____ & _____ (1982): Structural investigations of YPO_4, $ScPO_4$, and $LuPO_4$. *Inorg. Chem. Acta* **60**, 39-43.

MOËLO, Y., LASNIER, B., PALVADEAU, P., LÉONE, P. & FONTAN, F. (2000): La lulzacite, $Sr_2Fe^{2+}(Fe^{2+},Mg)_2Al_4(PO_4)_4(OH)_{10}$, un nouveau phosphate de strontium (Saint-Aubin-des-Châteaux, Loire-Atlantique, France). *C. R. Acad. Sc. Paris*, **330**, *Sér.* **II b**, 317-324.

MORDBERG, L.E., STANLEY, C.J. & GERMANN, K. (2001): Mineralogy and geochemistry of trace elements in bauxites: the Devonian Schugorsk deposit, Russia. *Mineral. Mag.* **65**, 81-101.

NI, YUNXIANG, HUGUES, J.M. & MARIANO, A.N. (1995): Crystal chemistry of the monazite and xenotime structures. *Am. Mineral.* **80**, 21-26.

NOVÁK, M. & SREIN, V. (1989): Chemical composition and paragenesis of wolframite from the Dolní Bory pegmatites, western Moravia, Czechoslovakia. *Acta Univ. Carolinae – Geol.* (the Čech Vol.) **4**, 495-500.

ORLANDI, P., PASERO, M. & VEZZALINI, G. (1998): Scandiobabingtonite, a new mineral from the Baveno pegmatite, Piemont, Italy. *Am. Mineral.* **83**, 1330-1334.

PETERSEN, O.V. & SECHER, K. (1993): The minerals of Greenland. *Mineral. Rec.* **24**, 4-65.

PUZENAT, L. (1939): La sidérurgie armoricaine. *Soc. Géol. et Minéral. de Bretagne, Mém., Tome* **IV**.

RAADE, G., FERRARIS, G., GULA, A., IVALDI, G. & BERNHARD, F. (2002): Kristiansenite, a new calcium – scandium – tin sorosilicate from granite pegmatite in Tørdal, Telemark, Norway. *Mineral. Petrol.* **75**, 89-99.

RASMUSSEN, S.E., JORGENSEN, J.-E. & LUNDTOFT, B. (1993): Refinement of the structure of YPO_4 by powder diffraction by three Rietveld programs. *Powder Diffraction* **8**, 164-167.

ROEDER, P.L. (1985): Electron microprobe analysis of minerals for rare-earth elements: use of calculated peak-overlap corrections. *Can. Mineral.* **23**, 263-271.

ROMANS, P.A., BROWN, L. & WHITE, J.C. (1975): An electron microprobe study of yttrium, rare earth, and phosphorus distribution in zoned and ordinary zircon. *Am. Mineral.* **60**, 475-480.

SABOURDY, G., SAGON, J.-P. & PASTIER, P. (1997): La composition chimique du xénotime en Limousin, Massif Central, France. *Can. Mineral.* **35**, 937-946.

SIGGEL, A. & JANSEN, M. (1990): Röntgenographische Untersuchungen zur Bestimmung der Einbauposition von seltenen Erden (Pr, Tb) und Vanadium in Zirkonpigmenten. *Z. Anorg. Allg. Chem.* **583**, 67-77.

Received March 11, 2002, revised manuscript accepted November 15, 2002.